Universiteit Utrecht

Faculteit Bètawetenschappen

Thermally induced non-linearity in a CROW photonic crystal

Bachelor Thesis

Hilbrand Wouters

Natuur- en Sterrenkunde

Supervisors:

prof. dr. A.P Mosk

K.L. Perrier MSc

June 13, 2018

Abstract

Photonic crystals are materials that interact with light similarly to the way electrons interact with regular ionic crystals. Their unique control over the propagation of light can be used in the fabrication of a wide range of optic devices. We study an InGaP coupled resonator optical wave guide (CROW) photonic crystal. The membrane contains three resonant cavities that exhibit non-linear behaviour, which can be attributed to both the Kerr effect and local heating of the material. The CROW is of interest as the cavities can function as an optic switch through their non-linearity. A brief overshoot of the steady state intensity is observed for off-on switches. This overshoot is used to demonstrate that the thermally induced non-linearity in the CROW is significant. The thermalisation time of a cavity is estimated to be roughly 4 microseconds, based on the decay of the overshoot.

Contents

1 Introduction **1**

2 Photonic crystals **2**

3 Set-up **4**

4 Experiment: Hysteresis in a single cavity **6**
4.1 Theory . . . 6
4.2 Experiments & Results . . . 7
4.2.1 Wavelength hysteresis . . . 7
4.2.2 Intensity hysteresis . . . 9
4.3 Discussion . . . 10
4.4 Conclusion & outlook . . . 10

5 Experiment: Thermalisation of a cavity **11**
5.1 Equipment response . . . 11
5.2 Method & data analysis . . . 12
5.3 Results . . . 13
5.4 Discussion . . . 14
5.5 Conclusion & outlook . . . 15

References **16**

A Bias controller user manual **I**

B Incomplete hysteresis loops **II**

C Delayed switches **II**

D Raw overshoot **II**

1 Introduction

All modern electronic appliances have been developed through precise engineering of the electric properties of their components. Their development was permitted by advances in solid state physics, exploiting the periodicity of the ionic structure of solids. This has given immense control over the propagation of electrons through well designed materials, leading to the development of transistors and diodes. Photonic crystals offer the capability to design optic systems similar to these electronic devices, because photon interactions with the photonic crystal can be controlled in a similar fashion to electron-crystal interactions. To this end, the photonic crystal must have a well engineered period structure.

Photonic crystals can be implemented in a wide range of optic appliances, like interferometers, lasers and amplifiers. They can be combined to create photonic integrated circuits, possibly leading to the development of optical computing and memory devices in the future. A key component for these systems is of course a switch, which can function as a transistor. In this thesis we use an experimental set-up to study a photonic crystal with an array of resonators that exhibit non-linear behaviour. The sample, known as a coupled resonator optical wave guide, is probed by an infra-red laser. Its resonators, or cavities, can switch between "on" and "off" states if the laser's wavelength is suitably changed, thus functioning as an optic switch.

Variation of the probe power is another method that can be used to force jumps between the cavities' on and off states. An electro-optic modulator was installed, giving accurate and high bandwidth controllability of the probe power. The device was used to investigate the non-linear effects of the crystal and study switches between stable states, using the Duffing equation as a model. This equation suggests the emergence of hysteresis at specific detuned wavelengths, through variation of the probe power.

The non-linear behaviour is predicted to be due to the Kerr effect and local heating by the high photon density in a cavity. The reaction time of the former effect is too short to allow independent observation, but the thermal influence occurs on a more observable microsecond time scale. A brief overshoot of the steady state intensity was observed when a cavity was switched on, decaying on a microsecond time scale. Experiments were performed to verify if this overshoot is a consequence of the thermal response of a cavity in the photonic crystal. Thus addressing the question: "Does local heating contribute to the non-linear behaviour of a CROW cavity?".

In this thesis we first explain the basic theory of photonic crystals and the sample we use. Next, the experimental set-up and electro-optic modulator are studied. Subsequently two experiments are performed and discussed. First we explore the non-linear behaviour of cavity, comparing the results with the Duffing model. In the second experiment we investigate the overshoot that occurs in an upward switch and review the role of heating in cavity's non-linearity. We finally present several improvements to the experiments and possible successive experiments exploiting the non-equilibrium response of the system.

2 Photonic crystals

Crystals are characterized by a periodic structure of atoms in a lattice. Interacting electrons will encounter a periodic potential within the crystal, a symmetry which restricts the wave function ψ of electrons to the following form

$$\psi(\mathbf{r}) = e^{i\mathbf{k}\cdot\mathbf{r}}u(\mathbf{r}), \tag{1}$$

where the function $u(\mathbf{r})$ is periodic in translations over the lattice vector, the wave function ψ is known as a Bloch state. This restriction of the wave function of electrons in crystal solids can be exploited to control electric properties of the material. Various geometries and compositions of crystals have allowed scientists to produce materials like insulators, semiconductors and conductors. Semiconductors for example have an energy band gap: meaning that there exist energy states which cannot be occupied by electrons in the solid. The band gap separates the valence band with occupied states and the conduction band with unoccupied states. Precise engineering of semiconductors has led to the development of transistors, the building block of all modern electronic appliances. Many more advances in technology can be attributed to the control of the behaviour of electrons in solids, by exploiting the periodic structure of these media.

Surprisingly, it is possible to design optic devices with similar properties. The primary condition for Bloch states to exist, is namely the presence of some appropriate periodic medium. For photons a suitable medium is a lattice in which there is periodicity in the dielectric properties. These materials, known as photonic crystals, can have symmetry in one, two and three dimensions and allow manipulation over the propagation of light. Photonic crystals can for example be designed as slow light devices, in which the group velocity of light is incredibly low. Having the ability to slow down light can be useful in information networks and even optical devices like lasers and interferometers[1]. They can also be designed with a photonic band gap, forbidding photons with certain wavelengths from propagating through the material[3]. This photonic band gap is a clear analogue with the energy band gap in a regular crystal. Defects in the photonic crystal can cause resonant modes to become available within the band gap. Well designed defects can therefore cause the crystal to function as an optical resonator[3].

The photonic crystal used in this thesis is a coupled resonator optical wave guide. It is a membrane of $Ga_{0.51}In_{0.49}P$ dielectric with a triangular lattice of air holes, as shown in Fig. (1). Within air holes

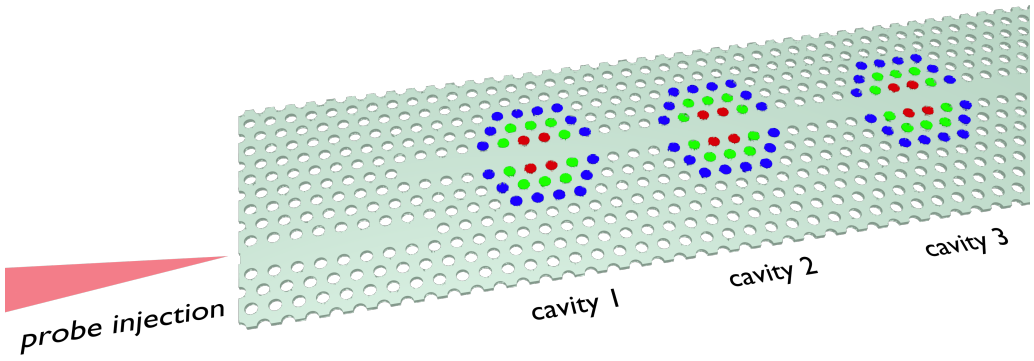

Figure 1: **Sketch of the sample.** A 180 nm thick photonic crystal membrane with a triangular lattice of air holes, the lattice vector is 485 nm in length. A line of holes is omitted to create a wave guide, transmitting the probe light. This wave guide is coupled to the three cavities, in which coloured circles indicate air holes that are shifted from the regular position. This intentional defect causes these regions to behave as resonators at specific frequencies.

the refractive index differs from the dielectric, thus forming a medium with periodic potential. The crystal is probed at the left hand side by a lensed fiber, which focusses infra-red laser light at the crystal, aligned such that the transverse-electric component (the plane of the electric field) is parallel to the plane in which the slab lies. The material contains three cavities, which function as high-Q optic resonators. Although the crystal is designed to contain most light, some of it will be leaked from the cavities at high intensity. Light will therefore scatter out of the crystal's plane, allowing it to be detected by a photo-diode. In this thesis we show that at low probe intensity the cavities respond linearly, but heating must be taken into account for higher probe power, causing non-linear effects. Non-linearity due to dependence of the refractive index on the electric field (the Kerr effect) is also predicted, as it is seen in similar systems[2]. The observed non-linear behaviour is therefore predominately of a classical nature, rather than quantum mechanical.

3 Set-up

The experimental set-up can be divided into three parts: the fiber branch, the box containing the sample and the free space branch. The light emitted by the tunable infra-red laser is transmitted through the fiber branch, containing several optic devices. A lensed fiber at the end of the fiber branch then probes the photonic crystal, which is mounted on a kinetic stage in a an air-tight nitrogen filled box at stable temperature. The nitrogen ambient gas prevents oxidation of the crystal's material. The free space branch contains mirrors, lenses and beams splitters, which provide an image of the sample, perpendicularly to its plane. This image can be focussed onto a photo-diode, to measure the out of plane scattering by the cavities. The image can also be pictured on visible and infra-red cameras to assist alignment. Finally the free space branch allows for pumping of the sample by external visible light lasers, causing local heating. This provides control over the resonant modes and the coupling of the cavities, but is not used in this thesis.

Electro-optic modulator
An electro-optic modulator (EOM) was placed in the fiber path and is used for intensity modulation of the probe signal. Its transmission is controlled by a wave generator, which applies a signal to an electrode on the modulator. Thus, the intensity of the probe can be modulated with any arbitrary signal produced by the wave generator (in this thesis a periodic triangle and pulses). The bandwidth of the modulator is on the order 10 GHz, which is sufficient for our experiments. A Mach-Zehnder interferometer, shown in Fig. (2), is the fundamental component of the device. In such an interferometer the input beam is split into two separate beams, which follow different paths and are later recombined. The phase of one of the paths is modulated, such that one can influence the degree of destructive interference upon recombination of the two paths[8].

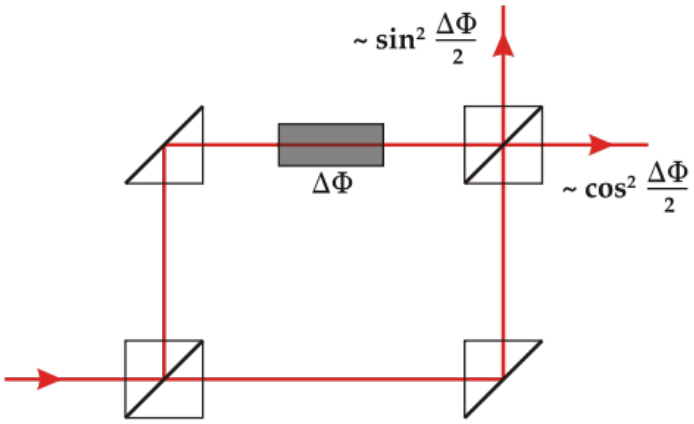

Figure 2: **Mach-Zehnder interferometer.**[1] An incident laser beam from the left is split into two beams, one of which passes through a phase modulator. The beams will interfere when they pass through the beam splitter in the top right. The two exit beams, one of which is the modulator's output, have different intensity due to a phase shift of the incident beams. The phase is modulated by a crystal of which the refractive index is dependant on the electric field applied by the wave generator.

The response of the modulator is wavelength and temperature dependent. So the optic response of the apparatus at a given wavelength is not predetermined. In practice, it is useful to know the modulator's response a priori. For example, when applying 0 Volt to the modulator's electrode, one would like to have 0% transmission(a situation we call 0 Volt bias). To achieve this, a bias controller is installed

[1] https:/nl.wikipedia.org/wiki/Mach-Zehnder-interferometer#/media/File:Mach-Zehnder_interferometer.svg

through which a small portion of the output signal is passed. This device calibrates the modulator at a set wavelength of the probe signal, such that the bias is locked at 0 Volt. This does not solve the issue of the possibility of bias drift, but wavelengths are only varied over a range of several nanometres in this thesis, which means that the chromatic dependence of the modulator is negligible. Also the thermal drift is negligible throughout measurements. A user manual is included in appendix A for the bias controller, as the manufacturer's manual is inaccurate.

The EOM's transmission is maximal at roughly 3.4 V after a calibration at the infra-red wavelengths used in this thesis. The electro-optic response is sinusoidal, so the transmission as a function of the applied voltage is $T(V) \approx \frac{1}{2} - \frac{1}{2}\cos\left(\frac{3.4\pi}{V}\right)$.

The implementation of the EOM in the fiber branch is shown in Fig. (3). Light is transmitted from the laser to the modulator, to which a wave generator and bias controller are attached. Any light transmitted by the modulator is directed into a 90/10 fiber splitter. The 90% branch is led into a circulator, which is installed such that it passes the light on to the sample. The circulator has the benefit of blocking any light that is reflected by the sample, as any reflected light will be directed into its third port (the dashed line) which is connected to a photoreceiver. This device can be used as a monitor similarly to the photo-diode for the out of plane scattering, but is not used in this thesis. The 10% branch of the fiber splitter is directed into another splitter, which divides the light into paths going to the bias controller and a photo-diode, the latter can be used to monitor the modulator's behaviour.

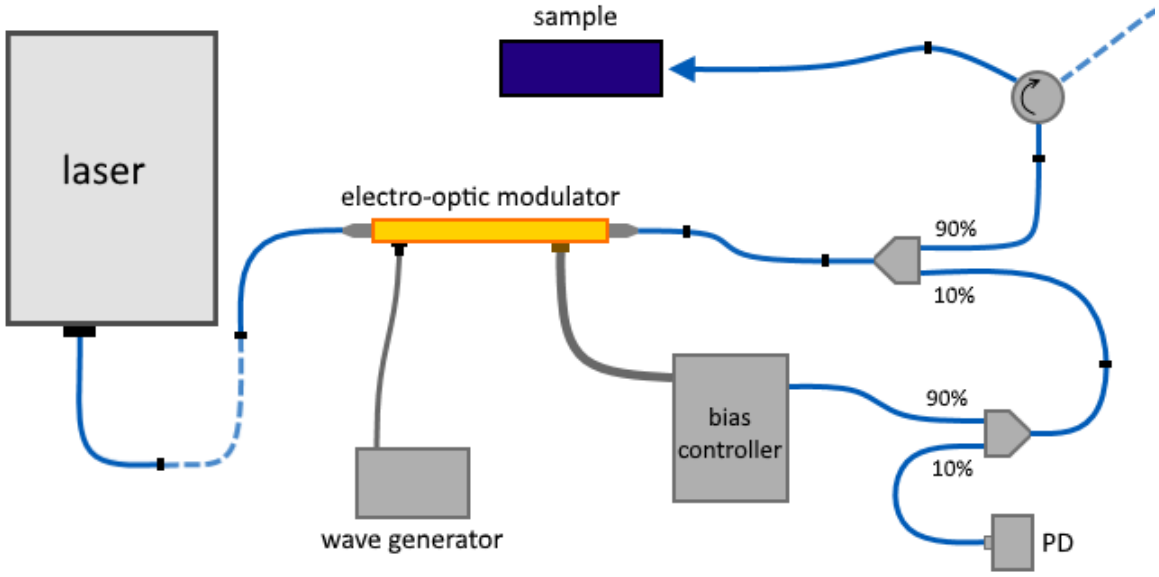

Figure 3: **Fiber branch of the set-up.** The blue lines depict fibers, the black rectangles indicate mating sleeves. The left-hand blue dashed line is a section of the fiber branch which contains several devices irrelevant to this thesis. The right-hand blue dashed line is connected to a photoreceiver, also not used in this thesis. Finally the grey lines that are drawn between the EOM and the wave generator and bias controller, are electric cables.

A portion of the injected light is lost through every optic component in the fiber branch, including the mating sleeves between different fibers. At 2.4 dB, the insertion loss of the modulator at maximum transmission is particularly high. The entire fiber path entails a total loss of approximately 90% at the end of lensed fiber, allowing a maximum output power of approximately 1 mW. The probe power is sufficient for the effects studied in this thesis, but does compromise the study of non-linear effects.

4 Experiment: Hysteresis in a single cavity

In this section we study the non-linear behaviour of a cavity, using relatively low probe powers and no external pumping, such that the coupling to other cavities is negligible. We first show how the Duffing equation predicts hysteresis at high probe intensity, and perform experiments to show that the cavity's response corresponds with this model.

4.1 Theory

A single cavity with small coupling can be described as a simple linear oscillator if we use sufficiently low probe power. Using x as a measure for the electromagnetic field's displacement in a cavity, the resulting differential equation is

$$\ddot{x} + \delta\dot{x} + \omega_0^2 x = \gamma\cos(\omega t), \tag{2}$$

where ω_0 is the resonant frequency of the system, δ is the 'damping' constant, which relates to the loss of energy, like out of plane scattering for the sample used in this thesis. The right hand term describes the driving at angular frequency ω. For high probe intensity this approximation fails, and we have to add a non-linear term, yielding the driven Duffing equation

$$\ddot{x} + \delta\dot{x} + \omega_0^2 x + \beta x^3 = \gamma\cos(\omega t). \tag{3}$$

This equation provides a suitable model for many non-linear systems, where the effects we study here are typically seen as well. This is primarily because the Duffing equation gives a good description for most pseudo-harmonic systems in which Hook's law is not exactly obeyed, like a pendulum or spring. Some electronic systems can also be described by the Duffing equation[5]. The non-linearity of a cavity was shown to be due to heating and the Kerr effect in a similar system[2]. That researched showed that the thermal influence was significantly larger, but the contribution of Kerr non-linearity is relevant on a shorter time scale. Both effects are likely present in the CROW as well.

To find an approximation of the systems response to a certain driving frequency and intensity, we make the ansatz $x(t) = a\cos(\omega t) + b\sin(\omega t) = r\cos(\omega t - \phi)$, where r must satisfy $r = \sqrt{a^2 + b^2}$. Substitution in Eq. (2) yields

$$\begin{aligned}\cos(\omega t)\left[-a\omega^2 + a\omega_0^2 + b\delta\omega - \gamma + \frac{3}{4}a^3\beta + \frac{3}{4}ab^2\beta\right] + \sin(\omega t)\left[-b\omega^2 + b\omega_0^2 - a\delta\omega + \frac{3}{4}b^3\beta + \frac{3}{4}a^2b\beta\right] \\ + \frac{\beta}{4}\left[\cos(3\omega t)(a^3 - 3ab^2) + \sin(3\omega t)(3a^2b - b^3)\right] = 0,\end{aligned} \tag{4}$$

where we have used the identity

$$\begin{aligned}x^3 = (a\cos(\omega t) + b\sin(\omega t))^3 =& \frac{1}{4}\big((3a^3\cos(\omega t) + a^3\cos(3\omega t) + 3a^2b\sin(\omega t) + 3a^2b\sin(3\omega t) \\ &+ 3ab^2\cos(\omega t) - 3ab^2\cos(3\omega t) + 3b^3\sin(\omega t) - b^3\sin(3\omega t)\big).\end{aligned} \tag{5}$$

Neglecting the $3\omega t$ terms in Eq. (4), the $\cos(\omega t)$ term and $\sin(\omega t)$ must each equal zero. Squaring, and some algebra, then yields

$$r^2\left(\left(\omega^2 - \omega_0^2 - \frac{3}{4}\beta r^2\right)^2 + (\delta\omega)^2\right) = \gamma^2. \tag{6}$$

This equation relates the steady state frequency response of a driven non-linear oscillator to the driving signal[4]. Here γ^2 is proportional to the intensity of the probe and r^2 is proportional to the system's

intensity, so the out of plane scattering for an optical cavity. In Fig. (4a) the blue line shows the linear behaviour (with $\beta = 0$) as a function of probe wavelength ω at a fixed probe intensity γ^2. For $\beta \neq 0$ numerical solutions to Eq. (6) are presented as well. We now observe a region where there are three solutions: the two solid lines are stable solutions, the dashed line can be shown to relate to unstable states[9].

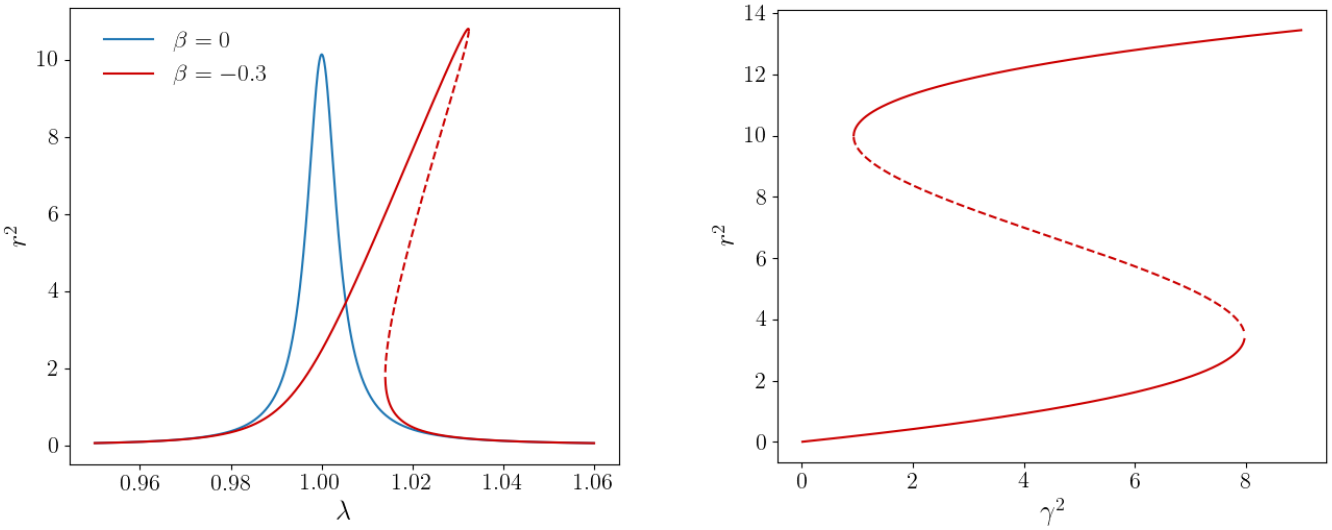

(a) Wavelength response, $\gamma = 1$.

(b) Intensity response, $\lambda = 1.03$.

Figure 4: **Steady state amplitude of the Duffing equation.** Numerical solutions to Eq. (6) for $\lambda_0 = 1$ and $\delta = 0.05$. In Fig. (4a) we show the linear ($\beta = 0$) and non-linear behaviour ($\beta = -0.3$) as a function of wavelength, in Fig. (4b) the response as function of probe intensity is shown for $\beta = -0.3$. In both non-linear cases we observe a region of bi-stability, where the red dashed line relates to unstable solutions.

Whether the non-linear cavity resides in the high or the low intensity state, depends on the history of the system. Take for example our non-linear system in Fig. (4a). When the initial wavelength is sufficiently small ($\lambda \lesssim 1.01$) and is then increased into the bistable region, the system will prefer the upper state. But there will no longer exist a stable state for $\lambda \gtrsim 1.03$ and the system will jump down to the lower state. If the wavelength is then decreased, it will remain in the lower state until it leaves the bistable region again. This phenomenon is known as hysteresis, and is a token effect in non-linear systems.

Solutions which display hysteresis due to variation of the probe intensity are also allowed by Eq. (6) when the wavelength is sufficiently detuned from λ_0. Such an hysteresis loop is displayed in Fig. (4b), again we have a bistable region. By applying a periodic signal (for example a sine or triangle) to the EOM one can vary the intensity to find a similar hysteresis loop at a detuned wavelength.

4.2 Experiments & Results

4.2.1 Wavelength hysteresis

We verify that the out of plane scattering of a single cavity with small coupling is approximated by the Duffing equation. To this end, we first probe a cavity at $20\,\mu$W and scan the wavelength over an

interval while recording the out of plane scattering.[2] Due to the low probe power, a linear description is valid, so we can omit β from Eq. (6) and get an analytic equation that relates the probe power signal to the intensity of the scattering

$$r^2 = \frac{\gamma^2}{\left(\frac{4\pi^2}{\lambda^2} - \frac{4\pi^2}{\lambda_0^2}\right)^2 + \left(\frac{2\pi\delta}{\lambda}\right)^2}. \tag{7}$$

In Fig. (5) we fitted this equation to the linear data (the blue solid line) to retrieve the cavity's linear parameters δ and λ_0. Next, we probed the cavity at high power[3], in the non-linear regime. The wavelength was scanned over an interval in both directions in Fig. (5). Hysteresis is observed and there exists a bistable region of approximately 2 nm. Numerical solutions to Eq. (6) are plotted by the blue dashed line, using the readily estimated linear parameters and an estimate for β.

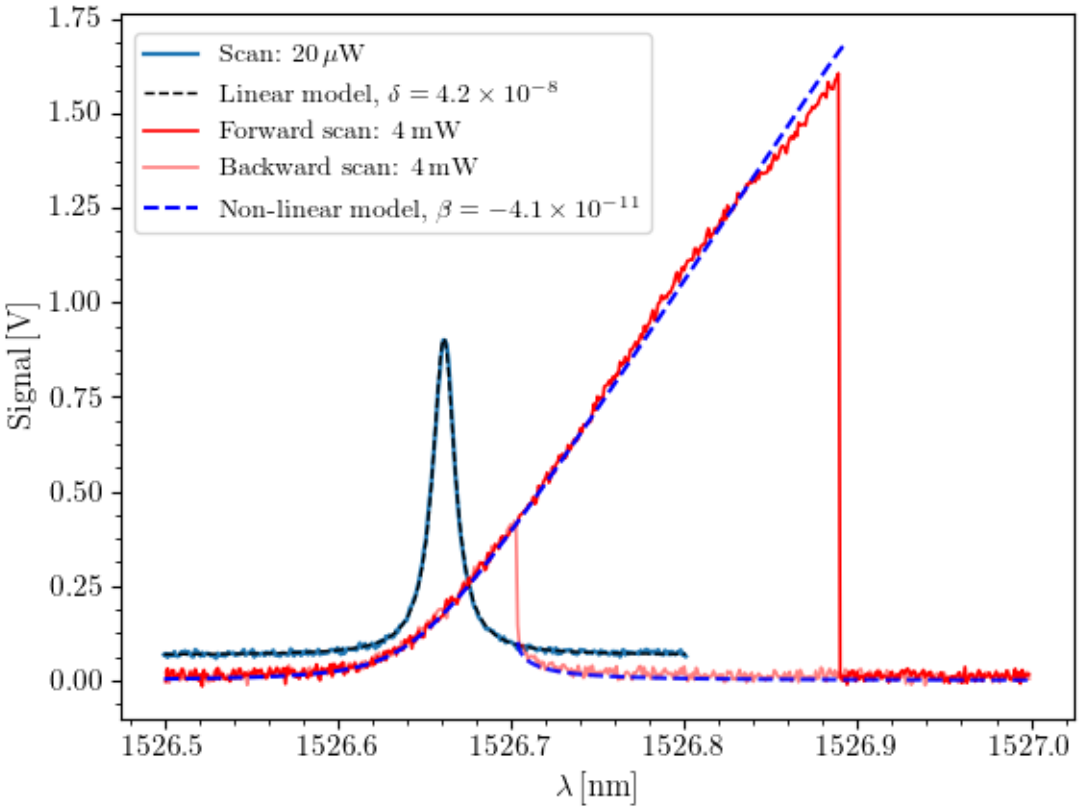

Figure 5: **Linear and non-linear behaviour of a single cavity.** The solid blue line is the mean of twenty scans probed at 20 μW, the black dashed line is a fit of Eq. (7), with $\delta = 4.2 \times 10^{-8}$, $\lambda_0 = 1526.661$ nm and $\gamma = 1.58 \times 10^{-10}$. The red line is a forward scan at 4 W (so for γ we now use $\sqrt{200}\gamma$), the opaque red line is a backward scan at the same probe power. The blue dashed line gives a numerical solution to Eq. (6) with the estimate $\beta = -4.1 \times 10^{-11}$. We observe hysteresis and a bistable region in the non-linear regime.

[2]Note that this is the power of the light emitted directly by the laser. The power at the tip of the lensed fiber is approximately 90% lower, due to losses in the fiber path and EOM.

[3]The signal at 20 μW was amplified one hundred times stronger than the 4 mW signal, hence the magnitude of the signals is comparable in Fig. (5).

4.2.2 Intensity hysteresis

To identify hysteresis due to intensity variation at fixed wavelength similar to Fig. (4b), we use the EOM to periodically vary the probe intensity. The solid lines in (Fig. 6) show the resulting hysteresis loops for five different detuned wavelengths. A triangular 100 Hz modulation signal was produced by the wave generator. The dashed lines are numerical solutions to Eq. (6), using the estimated parameters from the previous part. Note that we have corrected for a blue shift of 0.1 nm, which is due to partial evaporation of the water film on the sample due to heating. The reduced refractive index causes the resonant wavelength to decrease, but leaves the cavity's properties largely unaffected otherwise. Under particular circumstances it was observed that hysteresis loops were not consistently completed for every period of the probe laser, this is further studied in appendix B.

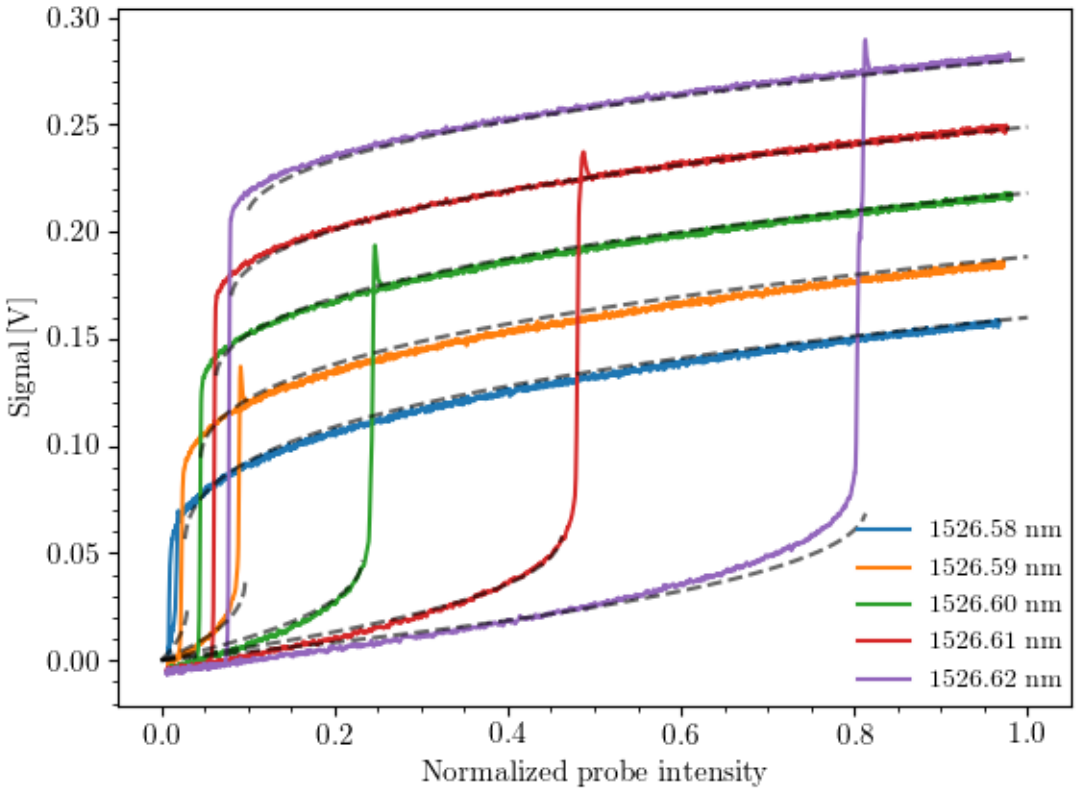

Figure 6: **Hysteresis loops at various detuned wavelengths.** Out of plane scattering at fixed wavelengths as function of probe power, which is periodically varied. We observe hysteresis loops which are run through anti-clockwise. The dashed lines show numerical solutions to Eq. (6) for each wavelength using the estimates $\delta = 4.2 \times 10^{-8}$ and $\beta = -4.1 \times 10^{-11}$.

4.3 Discussion

The Duffing model correctly predicts the non-linear behaviour for both the wavelength and intensity hysteresis. In both Fig. (5) and (6), a bistable region is observed, of which the size is reasonably estimated by the model. We also observe switches at the boundaries of the bistable region. The observed intensity is in good agreement with the prediction based on the estimated model parameters in both graphs. The small deviations from the observation, particularly in Fig. (6), can be attributed to drift of the resonant frequency, inaccuracies in the parameter estimates and effects that are not included in the model. No quantitative analysis was performed and the model was not tested at maximum probe power, so the limitations and accuracy of the model have not been investigated fully.

We do discern an interesting feature in Fig. (6): a small overshoot in the transition from the low intensity state to the high intensity state is visible for all wavelengths. We hypothesize that this effect is a feature of the thermally induced non-linearity of the photonic crystal, as it is out of thermal equilibrium briefly after the switch. The overshoot is studied in more detail in the next section.

4.4 Conclusion & outlook

We have shown that the Duffing equation is suitable to predict non-linear behaviour of a single optic cavity in a CROW photonic crystal. Hysteresis loops with a region of bi-stability were observed due to variation of both the probe power and wavelength. These hysteresis loops show that is possible to switch between both stable branches by power variation. An overshoot of the high intensity state was observed for upward switches. The limitations and accuracy of the model have not been investigated, so we are unable to predict the model's quantitative behaviour at a given wavelength.

Outlook
The sample used in this thesis consists of an array of three coupled cavities, of which the coupling can be altered by the probe intensity and external pumping. Strong coupling of two cavities can theoretically lead to multi-stability. Using the EOM to vary the probe intensity may help to identify and characterize these states, in addition to the already available method of tuning the wavelength of the laser.

5 Experiment: Thermalisation of a cavity

In the previous section an overshoot of the high intensity stable state was observed when an upward switch was made. We now hypothesize that this effect is due to the photonic crystal being out of thermal equilibrium for a brief period after the switch. When in resonance, the high density of photons will heat the cavity, which in turn locally heats the crystal until thermal equilibrium with the surrounding material and gas is reached. Throughout the thermalisation period, the lower temperature will cause a different optic response, which we observe as an overshoot. Note that heating due to high photon density is one of the predicted causes for the observed non-linearity, along with the Kerr effect, which is the refractive index's dependence on the electric field. Kerr non-linearity should have a response time which is orders of magnitude shorter than the thermalisation time, allowing us to distinguish between the two possible causes[2].

For a $Ga_{0.51}In_{0.49}P$ cavity with nitrogen as ambient gas, the 10-90% temperature rise time was estimated to be approximately $6\,\mu$s by Sokolov et al [7], based on COMSOL simulations. The thermal conductivity of the sample on which these simulations are based is approximately two-thirds compared to the thermal conductivity of the sample used in this thesis. Therefore we predict a shorter thermalisation time of roughly $4\,\mu$s. A rotationally symmetric temperature distribution is predicted with a half width at half maximum of approximately $3\,\mu$m in thermal equilibrium. Due to the high band-gap (1.85 eV) of $Ga_{0.51}In_{0.49}P$, it is believed that no two-photon absorption can contribute to the heating of the crystal. In this section, we study the overshoot that occurs for an upward switch, and show how the overshoot can indeed be attributed to an out of thermal equilibrium response.

In the main experiment the probe laser is turned on by applying a step function to the EOM. As the resulting phenomena happen on a very short ($\approx 1\,\mu$s) time scale, we first verify that the equipment response is sufficiently fast to record these signals. A deconvolution must still be performed to account for a slow amplifier response. Afterwards we present and discuss the results of the primary experiment.

5.1 Equipment response

In order to measure the response of the cavity to a fast switch in probe intensity the following equipment is used:

1. Wave generator: Which applies a step function of 0 to 3.3 V to the EOM, with a lead edge of 8.4 ns.
2. EOM: Modulates the probe signal.
3. Photo-diode: Records the out of plane scattering.
4. Femto current amplifier: Amplifies the photo-diode signal. Is used at (maximum) bandwidth of 500 kHz at 10^6 gain.
5. Oscilloscope: Records the amplifier output.

Based on the manufacturer's specifications, the current amplifier is the greatest constraint to the speed of the system response, as it is several orders of magnitude slower than any other device. This was also experimentally confirmed. We therefore conclude that the step response of the system is fully limited by the amplifier.

The step response, the blue line in Fig. (7), of the amplifier was measured by recording the scattering from the lensed fiber tip when applying a step function at a fixed non-resonant wavelength. The fiber was intentionally misaligned with the sample, to avoid the influence of reflections from cavities.

he oscilloscope is triggered by the wave generator at $t = 0\,\mu$s, but no significant response is visible until $0.2\,\mu$s, due to the relatively slow group velocity in the fibers and coaxial cables (a total of several metres). The response itself has a $10-90\%$ rise time of approximately $1.5\,\mu$s, which is a significant factor for the recording of switches, which show an overshoot on microsecond time scale as well. In the primary experiment, discussed in the next part, a deconvolution is therefore performed to account for the slow amplifier response. A deconvolution retrieves an input signal, after it passed through some filter, in this case the amplifier. If in the Fourier domain F is the input signal, H the transfer function (the impulse response) of the filter and G the output signal, then the most simple deconvolution method is

$$F = \frac{H}{G}, \tag{8}$$

which is accurate in the absence of noise[6]. Taking the inverse Fourier transform of F retrieves the original signal. More advanced deconvolution methods, like the Wiener deconvolution, incorporate the influence of noise, but are not used in this thesis.

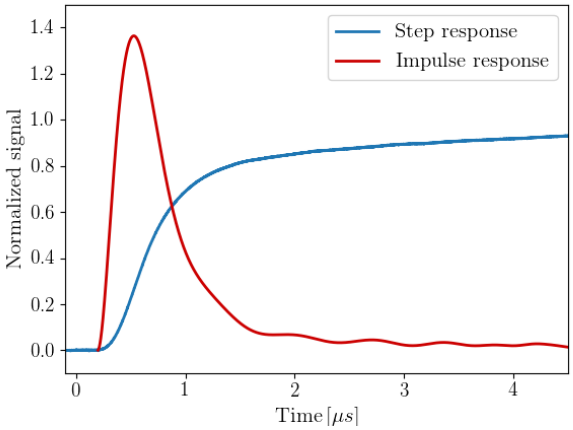

Figure 7: **Amplifier step and impulse response.** The blue line shows the normalized step response of the amplifier, averaged over 50 recordings. A 400 degree polynomial was fitted, of which the derivative is plotted by the red line.

A deconvolution requires a Fourier transform of the impulse response, which is shown in Fig. (7) as well. The red solid line shows an estimate of the impulse response made by fitting a 400 degree polynomial to the step response, and taking the first derivative of this fit.

5.2 Method & data analysis

Method

The crystal's response to an off/on switch was investigated by rapidly pulsing the probe intensity. As discussed in te previous part, this was done by applying a 0 to 3.3 V step function to the EOM with an edge of 8.4 ns. Multiple switches were recorded, with the intermediate time sufficient to return to thermal equilibrium. The modulator was calibrated with a bias at 0 V ahead of the experiment, to have maximum extinction. The out of plane scattering was detected by a photo-diode, amplified and then measured with an oscilloscope, which was triggered by the pulse of the wave generator. The experiment was performed in the non-linear regime, as maximum probe power was used. Several detuned wavelengths were studied, with intermediate steps of ten picometres. Wavelengths were chosen at or below the lower boundary of the bistable region, because within this region only the low intensity branch could be reached. The study of a small switch to a steady state with low intensity is definitely interesting, but was impractical due to poor signal to noise ratio. At the boundary of the bistable region, upward switches occurred after the low intensity state was first briefly inhibited. This effect, which itself provides evidence of heating in a cavity, is studied in more detail in appendix C.

Data analysis

A total of 540 recordings were made, with a $70\,\mu$s length and 2000 data points. As was previously discussed, some information is concealed in these raw recordings due to the slow amplifier step response. A basic deconvolution was therefore performed, using the estimated impulse response shown in Fig. (7). This simple operation is very sensitive to noise, amplifying any small perturbations. High bandwidth noise ($> 10\,$MHz) was therefore smoothed from the data with the SciPy implemented Savitsky-Golay filter. Averages and uncertainties were calculated over all smoothed and deconvoluted recordings.

5.3 Results

The deconvoluted and averaged switches are displayed in Fig. (8) for wavelengths between 1525.71 and 1525.76 nm. The modulator receives a step function at $t = 0\,\mu$s, after which we observe a brief overshoot of the steady state intensity. For all wavelengths, the peak intensity is over twice the steady state intensity. The decay of this overshoot is modelled by the black dashed lines, displaying fits with the function[4] $S(t) = \frac{T}{(t-t_0)^\alpha} + y_0$. In appendix D the raw data is plotted, without deconvolution. In the second column in Table (1) the estimated 90-10% decay times are listed, which are all close to the predicted $4\,\mu$s. No statistical analysis of these values is performed due to the small sample size. After this decay time we observe that the cavities reach thermal equilibrium, and intensity of the scattered light remains constant.

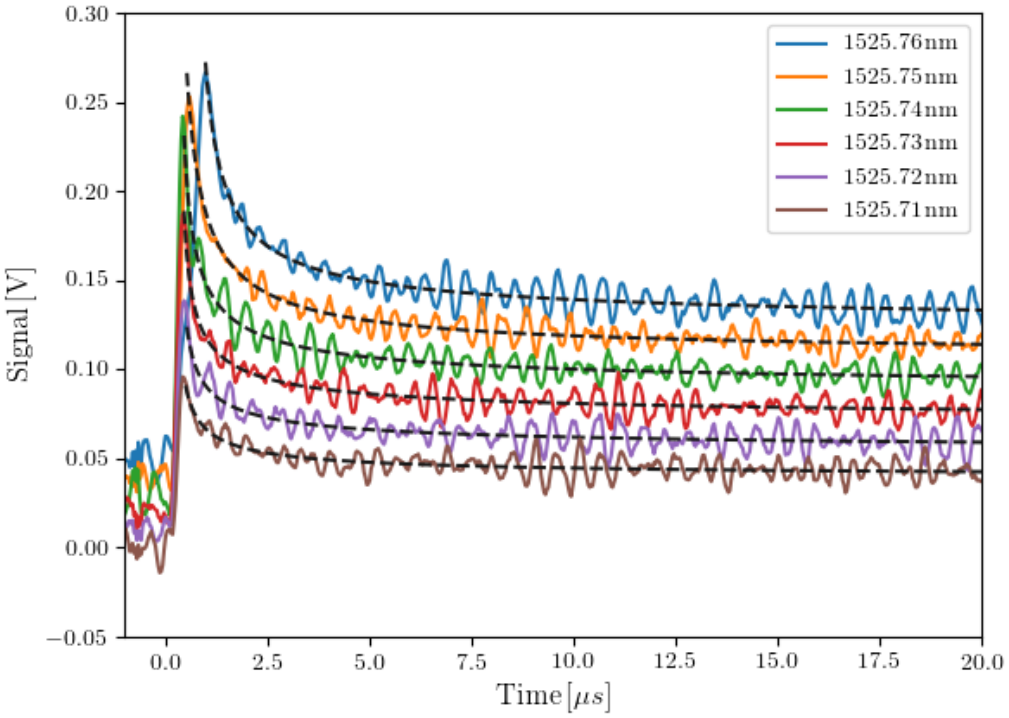

Figure 8: **Overshoot and decay at various wavelengths.** Response of a cavity as a function of time to a step function in probe intensity, deconvoluted and averaged over 90 recordings for six wavelengths. Plots at different wavelengths have been given a offset to aid presentation. Probe light is switched on at $t \approx 0\,\mu$s. Fits with $S(t) = \frac{T}{(t-t_0)^\alpha} + y_0$ are displayed by the black dashed lines. For each fit α lies between 0.54 and 0.79. No errors are displayed, but these were taken into account in the data analysis, giving values of the reduced chi-squared between 0.9 and 1.4.

A more detailed plot of the upward switch is shown in Fig. (9), in which the same data as in Fig. (8) is portrayed, but on a shorter time scale. Also the data is normalized based on the steady state intensity at each wavelength (so the y_0 term in the fit). We observe that both the relative peak height and the timing of these peaks is wavelength dependent. For the smallest wavelength the peak of the

[4]Note that this is an empirical model, we cannot provide any solid theoretical background. However, a $1/t^\alpha$ process is typical for diffusive systems.

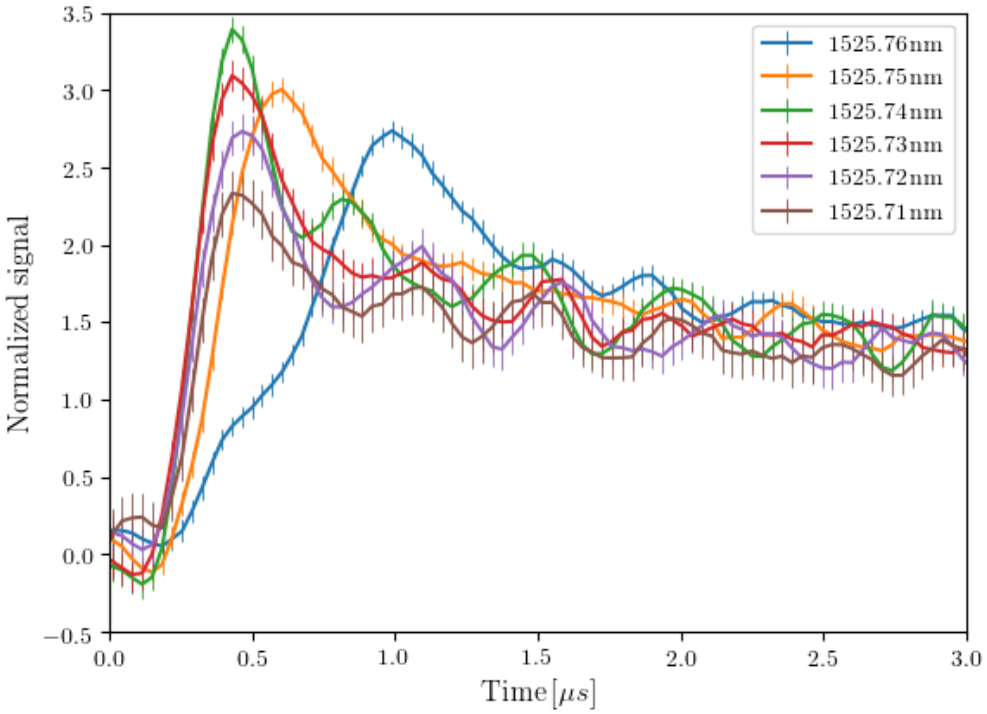

Figure 9: **Normalized overshoot at various wavelengths.** Detail from Fig. (8) normalized by the steady state intensity at each wavelength, including estimated error bars. The boundary of the bistable region is at $\lambda \approx 1525.75$, for smaller wavelengths there is only one stable state.

overshoot occurs earlier than for two largest wavelengths, which are at the boundary of the bistable region. The smaller wavelengths are in the region where there exists only one stable state, where increasing wavelength leads to a rise of the relative peak height. As we approach the bistable region we observe that the the peak height decreases, and the transition to the peak is slower. Corresponding values are listed in the third column of Table (1). In appendix C we study switches even closer to the bistable region, where upward switches are delayed by more than 100 μs.

Table 1: **Estimated decay time and overshoot height.** Based on the fits displayed in Fig. 8.

λ (nm)	90-10% decay time (μs)	Relative peak height
1525.76	5.27 ± 0.2	2.93 ± 0.07
1525.75	4.12 ± 0.14	3.16 ± 0.09
1525.74	3.65 ± 0.15	3.64 ± 0.09
1525.73	4.19 ± 0.25	3.32 ± 0.11
1525.72	4.7 ± 0.4	2.98 ± 0.13
1525.71	4.3 ± 0.4	2.48 ± 0.14

5.4 Discussion

From Fig. (8) we estimate 90-10% decay times between 3.65 to 5.27 μs, which is strikingly close to the 4 μs 10-90% temperature rise time we estimated based on the work by Sokolov et al. The fact that these two time scales are of similar order of magnitude provides evidence that the decay of the overshoot is indeed caused by the thermalisation of the cavity. An estimate or model for the local

temperature dependence of the optic response is however required to identify the exact connection between decay time and thermalisation.

Due to small sample size it is impossible to identify a clear trend between wavelength (or steady state intensity) and decay time, but all values in Table (1) are of similar order of magnitude. From Fig. (9) we deduce that for wavelengths outside the bistable region there exists a positive correlation between the steady state intensity and the relative peak height. However, for wavelengths at the boundary of the bistable region, the overshoot is significantly smaller. We suppose that this is caused by heating during the brief delay before the switch is made, reducing the local temperature deficit and therefore decreasing the peak height. Further improvements to the experiment may allow more accurate estimates of these relations.

Even though a deconvolution is performed, some of features of the switches may not be distinguishable as they occur on too short time scale. The peaks of the overshoots may for example have been truncated, regardless of the deconvolution. However, individual results can be compared, even though the full peak height can likely not be detected.

Deconvolution
Currently, a few issues occur in the implementation of the deconvolution. The complete lead edge of the impulse response could not be incorporated, but had to be shortened by $\approx 0.1\,\mu$s to produce a workable signal to noise ratio. Smoothing is also necessary, as the basic deconvolution method does not take into account noise. Nevertheless, noise is still amplified in the deconvoluted data. In a subsequent experiment more advanced deconvolution techniques may be applied to cancel the influence of noise, and avoid the need to restrict the impulse response.

Periodic noise
In all experiments with a low signal to noise ratio, periodic background noise of unknown origin was encountered. The primary component has a frequency of approximately 200 kHz, but the signal has dozens of constituents with frequencies up to several megahertz. In Fig. (8) both the 200 kHz and a 2 MHz components are visible, which should have been prevented by averaging over multiple recordings. Curiously, the noise therefore appears correlated, which is neither predicted nor explicable. Further research, where more data is acquired at a higher resolution, should indicate if the noise can be averaged out, or if it really is correlated.

5.5 Conclusion & outlook

An overshoot of the steady state intensity for off-on switches was observed. We found strong evidence that this overshoot is caused by the cavity briefly being out of thermal equilibrium after a switch. Heating therefore plays a significant role in the non-linear response of CROW photonic crystal, possibly in combination with Kerr non-linearity. Several estimates of the 90-10% decay time of the overshoot lay within the interval 3.65 to 5.27 μs, and are therefore in correspondence with the predicted 4 μs based on simulations by Sokolov et al [7]. Pre-heating in advance of switch at wavelengths at the boundary of the bistable region was observed, causing a reduction of the relative overshoot height.

Further research is required to find the correspondence between steady state intensity and decay time, as well as relative peak height. Predicting the influence of local heating on the optic response of a cavity will also help to find the exact thermalisation time, and possibly the shift in temperature. This may help to identify whether two-photon absorption is a significant factor in the heating of a cavity. The thermal non-linearity can also be influenced by changing the ambient gas from nitrogen to helium, which has a higher thermal conductivity. It is expected that the thermalisation time should then decrease by a factor of three.

Outlook
The experiments have demonstrated the ability to vary the probe power and acquire data on a time

scale shorter than the thermalisation time. This allows one to study the crystal's behaviour out of thermal equilibrium, which may reveal more interesting phenomena and give insight in the dynamics of the material. Several experiments are imaginable, using the EOM at high frequencies. For example, one could reproduce the hysteresis loops shown in Fig. (6), where the probe power is varied at frequencies of the order 100 kHz. One would likely observe a retardation of the cavity's response, causing both the upward and downward shift to be delayed, thus increasing the area covered by the hysteresis loop. Similarly, one may find interesting non-equilibrium behaviour when adding Gaussian noise with a bandwidth of > 100 kHz. All these experiments can be combined with wavelength scans, and external pump lasers may also be used to heat the crystal, which should influence the observed effects.

As has been noted, the current experiment may be improved by better data acquisition and analysis. Further detail regarding the thermalisation of a cavity should be identifiable by making smaller steps in intensity, rather than a zero to maximum intensity switch. The pre-heating caused by non-zero power in the cavity, should result in similar behaviour to the delayed jump at $\lambda = 1525.76$ nm in Fig. (9).

In the present study, the decay of an overshoot was primarily investigated. The rise in intensity should however also harbour information regarding the reaction time of the system, and is therefore of interest as well. As the rise is at least an order of magnitude faster than the decay, a higher bandwidth amplifier would be required.

References

[1] T. Baba. Slow light in photonic crystals. *Nature Photonics*, 2, 2008. p. 466.

[2] V. Eckhouse, I. Cestier, G. Eisenstein, S. Combrié, G. Lehoucq, and A. D. Rossi. Kerr-induced all-optical switching in a gainp photonic crystal fabry-perot resonator. *Opt. Express*, (8), 2012. p. 8533.

[3] J. Joannopoulos, S. Johnson, J. Winn, and R. Meade. *Photonic Crystals: Molding the Flow of Light*. Princeton University Press, 2008. ISBN 978-0-691-12456-8. p. 74-75, 78-82.

[4] D. W. Jordan and P. Smith. *Nonlinear Ordinary Differential Equations - An introduction for Scientists and Engineers*. Oxford University Press, 4 edition, 2007. ISBN 978-0-19-920824-1. p. 225-229.

[5] I. Kovacic and M. Brennan. *The Duffing Equation: Nonlinear Oscillators and their Behaviour*. John Wiley & Sons, 2011. ISBN 978-0-470-71549-9. p. 25-51.

[6] J. Proakis and D. Manolakis. *Digital Signal Processing: Principles, Algorithms, and Applications*. Prentice-Hall International, 1996. ISBN 0-13-394338-9. p. 355-359.

[7] S. Sokolov, J. Lian, E. Yüce, S. Combrié, G. Lehoucq, A. D. Rossi, and A. P. Mosk. Local thermal resonance control of gainp photonic crystal membrane cavities using ambient gas cooling. *Applied Physics Letters*, 106, 2015. p. 171114-171116.

[8] K. P. Zetie, S. F. Adams, and R. M. Tocknell. How does a mach-zehnder interferometer work? *Physics Education*, 35(1), 2000. p. 47-48.

[9] Z.Wu, R. Harne, and K. Wang. Excitation-induced stability in a bistable duffing oscillator: Analysis and experiments. *Journal of Computational and Nonlinear Dynamics*, 10, 2015. p. 11016-11017.

A Bias controller user manual

Introduction

The YY Labs Mini-MBC-4 bias controller locks the bias position of an electro-optic modulator at null, meaning that after a calibration there is minimum transmission of the modulator when zero volt is applied to its RF-port. The bias controller must be connected to three of the four pins on the modulator. One of those is a grounding, the other are the Bias 1 and Bias 2 pins. Bias 1 is for course control and is used to do a rough minimisation of the transmission, after which Bias 2 is used to do fine tuning, thus further increasing the extinction ratio.

In this manual we focus only on the front panel, as the rear panel is for pulsed lasers. Any text in ***Bold*** refers to the name of an element on the front panel.

Note that on several topics the *YY-labs* user manual differs from this one, as the companies' manual is inaccurate.

The Front Panel

1. Optic ports: Output of the modulator should be connected to the ***IN*** port. The ***OUT*** ports transmits the signal, but scrambles the polarisation, so should not be used for purposes the polarisation should be maintained. Rather, a small portion of the modulator output should be directed into the bias controller in this case, while the output is closed off. Note: only FC/PC connectors must be used.
2. The ***Bias Status*** segment: Containing two LED's, the red ***Reset*** button and the ***Cal*** switch.
3. The ***fine tuning*** segment: Containing an ***auto*** switch, ***dither*** switch and another red ***reset*** button. Both the ***auto*** switch and red ***reset*** button have *no apparent function*. So whenever we refer to a reset button in the future, we refer the ***Reset*** button in the ***Bias status*** segment.
4. A green on/off switch

Calibration

A calibration is initiated whenever the bias controller is turned on, or when the ***Reset*** button is pushed and released. During a calibration, which takes about 90 seconds, the laser must be stable and no signal should be applied to the modulator's RF-port. If the bias controller is first switched on, a calibration must be done with both course control (pin 1) and fine tuning (pin 2). To do so, the ***Cal*** switch must be up. The bias will drift slowly after a calibration, causing the electro-optical response to change. This will also occur if the wavelength of the laser is altered. If a small drift occurred, one can do a calibration with only fine tuning by flicking the ***Cal*** switch down and pushing the ***Reset*** button next to it. Again, the RF-signal must be off and the laser stable. The range of the fine tuning is sufficient to correct for changes in wavelength of more than 50 nm between subsequent calibrations, so rough control is unnecessary after the first calibration. When the calibration is finished, make sure that the ***dither*** switch is down before applying an RF-signal. There is no need to recalibrate if the power of the laser is altered.

The green and red LED's provide information on the status of the bias controller. During a calibration the green LED will flash with various frequencies, once finished it will remain stable. If the red LED flashes there is something wrong, likely the light signal is too weak. It will also flash if an APC connector is used on the IN port. After the red LED has flashed, the green LED may start flashing

with a frequency of approximately 1 Hz, in that case the problem has not been solved and no calibration can be done.

Calibrating with the *dither* switch

When the ***dither*** switch is up, the bias controller will always attempt to minimize the transmission, even if an RF-signal is applied. The switch should therefore always be down when the RF-signal is on, to make sure that the bias controller remains passive after a calibration. However, when the bias has drifted, flicking the switch up will very quickly return transmission to its minimum. So one can do a fast 'calibration' by turning the RF-signal off and flicking the ***dither*** switch up and down. Since the precise mechanism behind this and effects of doing it repeatedly are unknown, one should have some reserve in doing this. Although taking considerably longer, doing a full calibration (with only fine tuning) is probably the preferred option.

B Incomplete hysteresis loops

The hysteresis loops shown in Fig. (6) could only be produced in a small ($\approx 0.50\,\mathrm{nm}$) wavelength interval for the cavity that was studied. On the boundaries of this interval, hysteresis loops would not be consistently completed for every period of the probe light, as in shown in figure 10. Here we see that for two cycles, no upward switch is made. The effect, which appears to be completely stochastic, is likely due to small variations in laser intensity or instabilities in the properties of the crystal. A thorough analysis of the statistics of this effect may reveal information regarding the stability of the crystal, if other instabilities can be excluded. The hysteresis loops that were discussed in section 4 all showed regular behaviour, meaning that intensity switches were made in each recorded cycle.

C Delayed switches

In section 5 we noted that for wavelengths at the boundary of the bistable region, a switch to a high intensity state was only made after a brief wait time. Fig. (11) shows four switches at three separate wavelengths. Again, the probe light is switched on at $t = 0\,\mu\mathrm{s}$, but no immediate jump is made. Rather the system resides in a state with low intensity, and quick switches are made after 80 to 400 μs. We observe that for smaller wavelengths, the upward jump on average occurs earlier than for the longer ones, and the standard deviation of the delay appears much smaller. During the delay, the cavity slowly heats, causing a shift of the boundary of the bistable region. As the wavelength effectively drifts out of this region, an upward switch eventually occurs. This behaviour is therefore additional evidence that heating of the cavity is a significant factor in its non-linear behaviour and its optic response. The variability of the delay time is likely caused by similar instabilities as the incomplete hysteresis loops discussed in appendix B. A statistical study is therefore of similar interest.

D Raw overshoot

In Fig. (12) we display the data acquired in the experiment in section 5, without a deconvolution. The same basic features are visible, but less detail regarding the relative peak height and the corresponding timing can be deduced. Note that periodic noise is visible in this figure as well.

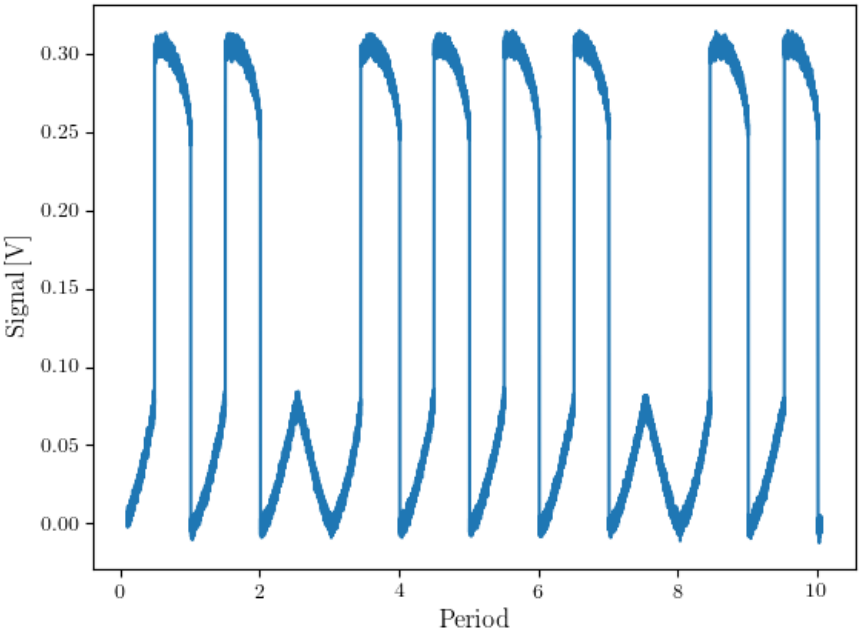

Figure 10: **Incomplete hysteresis loops.** Out of plane scattering as a function of the period of the variation of the probe light at $\lambda = 1526.69$. The 0.1 Hz signal applied to the wave generator was triangular, such that the modulator's relative transmission was 7% at minimum. Two periods are depicted where no upward switch is made, the other periods display hysteresis similar to Fig. (6).

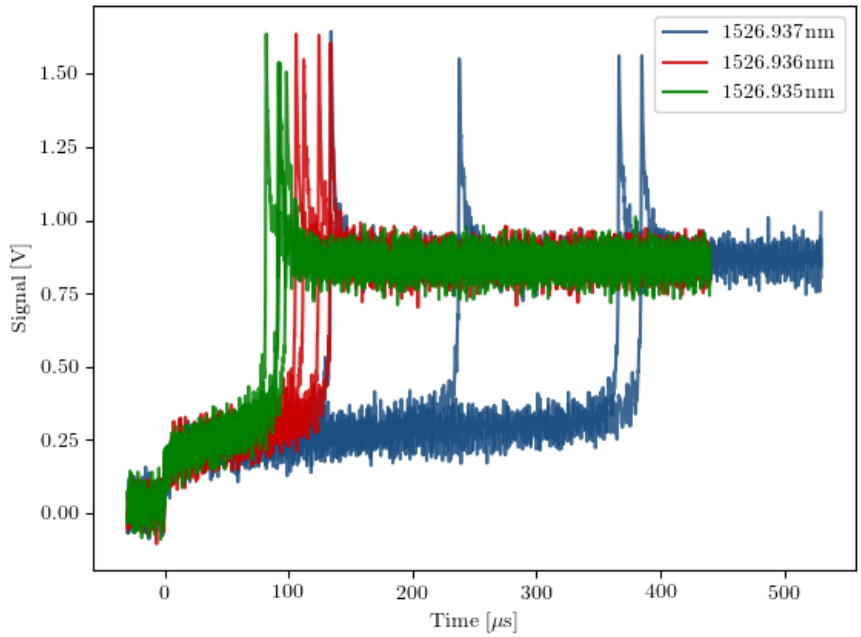

Figure 11: **Delayed switches.** At each wavelength three recordings (taken with brief intervals) are displayed, where the probe light is turned on at $t = 0\,\mu$s. The wavelengths are at the boundary of the bistable region. We observe a variable delay between the off/on switch of the probe and the jump to the high intensity state. Both the duration of the delay and the standard deviation increases as the wavelength is increased further near the bistable region.

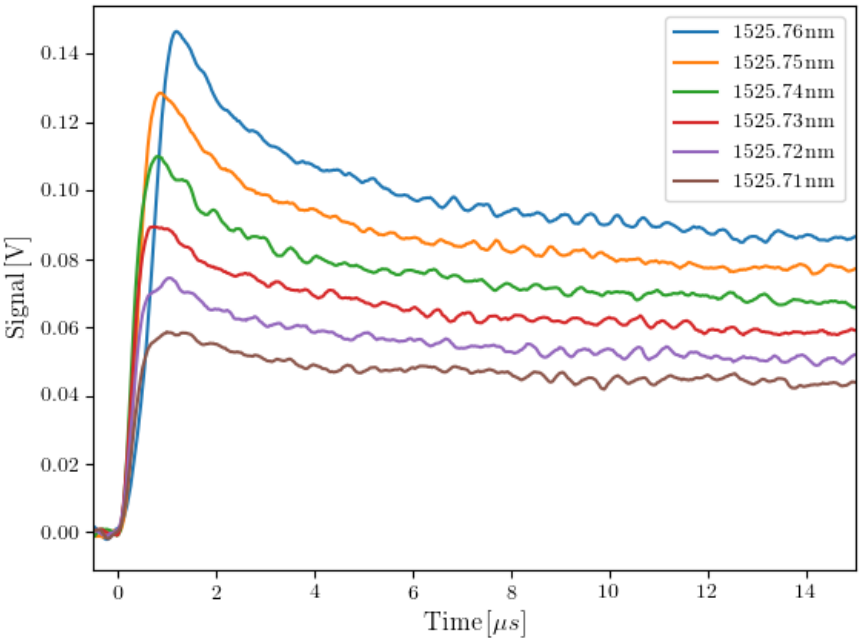

Figure 12: **Overshoot without deconvolution.** This plot uses identical data as in Figs. (8) and (9), but no deconvolution or normalization is performed. Averages of 90 recordings are calculated at each wavelength.